Pharm Res (2012) 29:97–109
DOI 10.1007/s11095-011-0514-6

RESEARCH PAPER

Solid Lipid Nanoparticles Loaded with Anti-microRNA Oligonucleotides (AMOs) for Suppression of MicroRNA-21 Functions in Human Lung Cancer Cells

San-Jun Shi • Zhi-Rong Zhong • Jie Liu • Zhi-Rong Zhang • Xun Sun • Tao Gong

Received: 28 March 2011 / Accepted: 10 June 2011 / Published online: 6 July 2011

ABSTRACT

Purpose Literature has highlighted the practical use of solid lipid nanoparticles (SLNs) in research, but few reports have combined SLNs with miRNA-based therapy. We aimed to prepare SLNs to load anti-miRNA oligonucleotide (AMO) for miRNA-based therapy *in vitro*.

Methods SLNs were employed to encapsulate AMO by a solvent diffusion method, and then the properties of AMO-CLOSs (cationic lipid binded oligonucleotide (AMO)-loaded SLNs) were characterized. We studied cellular uptake and activation properties of AMO-CLOSs in A549 cells, including antisense efficiency, cell migration and invasion.

Results AMO-CLOSs were 187 nm in size and 46.6 mV in zeta potential with an approximately toroid morphology in the TEM image. AMO-CLOSs uptake by A549 cells was increased significantly higher and more effective than free AMO. Further results demonstrated that AMO-CLOSs showed high antisense efficiency of microRNA-21 and subsequently decreased the proliferation, migration and invasion of tumor cells.

Conclusions These findings suggest that AMO-CLOSs represent a potential new approach for carrying anti-miRNA inhibitors for cancer therapy.

KEY WORDS anti-miRNA oligonucleotide (AMO) · antisense efficiency · microRNA-21 · microRNA-based therapy · solid lipid nanoparticles

S.-J. Shi • Z.-R. Zhong • J. Liu • Z.-R. Zhang • X. Sun (✉) • T. Gong (✉)
Key Laboratory of Drug Targeting and Drug Delivery Systems
Ministry of Education, West China School of Pharmacy
Sichuan University
Chengdu, Sichuan 610041, People's Republic of China
e-mail: xunsun22@gmail.com
e-mail: gongtaoy@126.com

ABBREVIATIONS

AMO	anti-miRNA oligonucleotide
AMO-CLOSs	cationic lipid binded oligonucleotide-loaded SLNs
DDAB-AMO	DDAB-binded AMO complexes
miR-21	microRNA-21

INTRODUCTION

MicroRNAs (miRNAs) are endogenous 18–24 nucleotide RNAs that function as triggers of the RNA interference pathway that suppresses gene expression by binding to their target mRNAs, preferentially to the 3′-untranslated region (3′-UTR) with a partial base-paring mechanism (1). Recently, miRNAs have been acquainted as a novel class of important gene-regulatory molecules involved in many critical biological functions such as cell proliferations, developments, cellular functions and even tumorigenesises (1–4). In many solid tumors, some miRNAs are overexpressed or amplified, suggesting that these miRNAs negatively regulate tumor suppressor or proapoptottic genes and play a spiffy role as oncogene in tumor pathogenesis and progression (2,5,6). In agreement with this mind, multiple studies have introduced anti-miRNA oligonucleotide (AMO) to depress the activities of this kind of miRNA in cancer cells, which have been proven to be highly effective (7–11). With the gradual deepening of research, AMO inhibition of microRNA functions is an important tool for uncovering miRNA biology and is considered a potential therapeutic approach for miRNA therapy of human diseases, e.g. cancer.

MicroRNA-21 molecule (miR-21) is one of the most prominent miRNAs implicated in the genesis and progression of human cancers (6). In human lung cancer A549 cell line, overexpression of miR-21 both causes cell proliferation and inhibits cell apoptosis (12). Reduced miR-21 expression is significantly associated with shortened activities of cancer cell proliferation and growth *in vitro* (7,12,13). These results support a functional role for miR-21 in mediating cell proliferation, migration and invasion, and suggest a mechanism by which overexpression of miR-21 may contribute to tumor metastasis in lung cancer. Thus, anti-miR-21 oligonucleotide (anti-miR-21 AMO), targeting to miR-21, is raising the hope for miRNA-based cancer therapy.

However, naked AMO is a nuclease-labile and hydrophilic polyanion with poor biomembrane permeability. The efficiency of such anti-sense oligonucleotides (ASO) therapy has been increased by recent advances in the bio-stability of ASO, with 2′-O-methyl or 2′-O-methoxyethyl modifications (14), but this reduces the specificity and the high affinity to the target mRNAs (15) and does not overcome the challenge of efficient delivery of ASO into cells. A nanoparticulate delivery system would change these disadvantages of ASO or AMO with improved stability and delivery efficiency.

Over the last few decades, SLNs, as a newly developed submicron drug delivery system, were introduced as a particular kind of colloidal system with a mean diameter from 10 to 1,000 nm (16). SLNs were made from natural or synthesized lipids which have excellent biocompatibility or biodegradability (17). The main peculiarities of SLNs include the protection of incorporated labile drugs from degradation (18), controlled drug release (16), rapid uptake by cell lines due to the affinity with the cell membrane (19,20), and possible targeting by the suitable chemical modification. Moreover, the availability of a suitable large-scale production method makes SLNs quite promising as a drug delivery system. So far, Lee *et al.* (21), Choi *et al.* (22), Vighi *et al.* (23) and Pozo-Rodíguez *et al.* (20) have prepared SLNs to carry DNA for gene delivery with some progressive results. Nevertheless, the carrying of AMO by SLNs and the combination of SLNs with the miRNA-based therapy have never been reported by publications.

With the comprehended advantages of AMO and SLNs, our study aimed to incorporate the functional AMO into cationic SLNs (named AMO-CLOSs) for silencing up-regulated miR-21. Moreover, the characteristics of AMO-CLOSs as well as their uptake behavior in A549 cells were investigated. After AMO-CLOSs were internalized into cells, AMO was released from nanoparticles to target the mature miR-21 and subsequently induced cell apoptosis (Fig. 1). This AMO delivery system was then assessed in lung cancer cells.

MATERIALS AND METHODS

Materials

Glyceryl monostearate (GMS) and soy phosphatidylcholine (SPC) were purchased from Taiwei Pharmaceutical Co., Ltd. (Shanghai, China); cholesterol (Chol) was obtained from Boao Biotech Co., Ltd. (Shanghai, China). Dimethyldioctadecylammonium bromide (DDAB), 3-(4, 5-dimethylthiazol-2-yl)-2, 5-diphenyltetrazolium bromide (MTT), propidium iodide (PI) and trypsin were from Sigma (USA). ECM gel from engelbreth-holm-swarm mouse sarcoma was supplied by Sigma-Aldrich (USA), as well. Lipofectamine™ 2000 was purchased from Invitrogen. Bulge-loop™ miRNA qPCR Primer Set was purchased from RiboBio (Guangzhou, China). FAM-labeled 22-mer oligonucleotides, oligonucleotides complementary to miRNA-21 (AMO), 3 nt mismatches of AMO to miR-21 and nonsilencing controls were ordered from Sangon Biotech Co., Ltd. (Shanghai, China). All other used reagents were of analytical grade.

Cell Lines and Culture Conditions

Human lung adenocarcinoma cell line A549 was obtained from American Type Culture Collection (ATCC) and was cultured in RPMI-1640 medium (HyClone, USA) supplemented with 1% penicillin/streptomycin, 2 mM glutamine and 10% fetal bovine serum (FBS; Minhai, China), in a humidified atmosphere containing 5% CO_2 at 37°C.

Preparation of DDAB-Binded AMO Complexes (DDAB-AMO)

DDAB-AMO was prepared by bligh and dyer extraction method (24). The monocationic lipid DDAB and AMO (FAM-labeled) were solubilized in a Bligh and Dyer monophase consisting of chloroform/methanol/water (1: 2.1: 1). Briefly, AMO (10 μg) and DDAB (30–120 nmol) were combined in the monophase by adding 525 μL methanol. The monophase mixture was subsequently partitioned into two phases by addition of 250 μL each of chloroform and water. The samples were mixed vigorously by vortexing for 1 min and centrifuged at 1,000 *g* for 10 min at room temperature. The upper aqueous phase and the lower organic phase were separated, respectively, and the amount of AMO in each phase

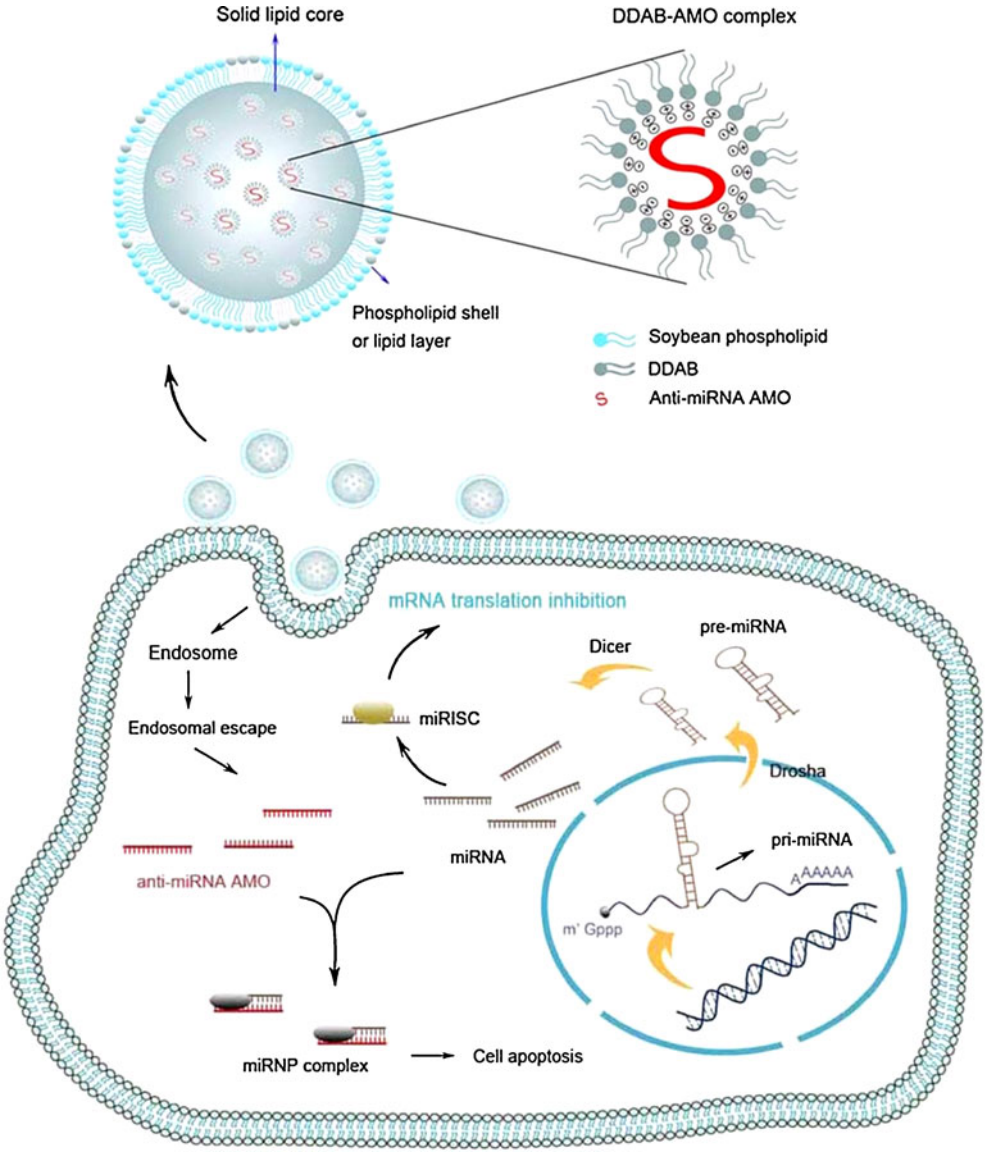

Fig. 1 Schematic representation of cationic lipid-binded AMO-loaded SLNs (AMO-CLOSs) for delivery of anti-miR-21 AMOs into cancer cells.

was determined by RF-5301 PC fluorospectrophotometer (Shimadzu, Japan).

Formulation of Cationic Lipid-Binded Oligonucleotide-Loaded SLNs (AMO-CLOSs)

Solid lipid nanoparticles (SLNs) loaded with anti-miR-21 oligonucleotide (AMO) (AMO-CLOSs) were prepared by a solvent diffusion method (25) with a minor modification. To improve the incorporated efficiency of hydrosoluble AMO in SLNs, initially, DDAB-AMO complex with high lipophilicify was obtained as mentioned above. Then, 100 μL DDAB-AMO complex containing 540 nmol of DDAB and 60 μg of AMO was added to 0.9 mL ethyl acetate solution containing 4 mg glyceryl monostearate (GMS), 1 mg soy phosphatidylcholine (SPC) and 1 mg cholesterol (Chol) to form oily phase, subsequently, which was quickly dispersed into 2 mL 0.1% poloxamer 188 solution under sonication (40 W, 15 s) for leading to an O/W emulsion. The organic solvent was removed completely for 4 h by the rotary evaporator.

Characterization of AMO-CLOSs

Particle size and zeta potential were measured in PBS (pH 7.4) by photon correlation spectroscopy (PCS) (Malvern zetasizer Nano ZS90, UK). The morphology of AMO-CLOSs was observed by transmission electron microscopy (TEM) (H-600, Hitachi, Japan). For the encapsulation efficiency measurement, the non-entrapped AMO in the aqueous phase was separated by ultrafiltration method (3,000 g, 30 min). FAM-

labeled AMO was used to enable fluorometric measurements of AMO concentration. The entrapment efficiency was obtained based on AMO concentration in the particles divided by AMO concentration added.

Stability of AMO in the Presence of Phosphodiesterase

Free AMO and AMO-CLOSs were incubated in parallel with 2.5 units of DNase I at 37°C for 5 min, 0.5 h, 1 h and overnight, respectively. At the desired times, the enzymatic digestion was terminated with 5 μL 0.5 M EDTA solution. Afterwards, AMO was released from SLNs by adding TritonX-100 to a final concentration of 1% and heparin to a final concentration of 0.9%. The hybridization capability and the stability of AMO were determined using a fluorescence temperature cycler (iQ™5, Bio-Rad, USA) (26). In brief, 20 ng of AMO were incubated with its complementary sense oligonucleotide in a 1: 1 ratio in presence of SYBR Green I diluted in the buffer (100 mM Tris-HCl, 100 mM NaCl and 14 mM $MgCl_2$). The two oligonucleotide strands formed a duplex because of the base complementarity. SYBR Green I was bonded to the double-strand structure, resulting in emitting a strong fluorescence signal which is proportional to the hybridization capability. Then a melting curve dependent on the changes of the intensity of fluorescence signal was acquired by the slow heating of the duplex from 37 to 95°C at a speed of 0.5°C/s.

Cellular Uptake of AMO-CLOSs in A549 Cells

For the visualization of (FAM-labeled) AMO-loaded SLNs internalization by tumor cells, A549 cells were seeded in a 24-well culture plate and allowed to attach overnight in RPMI 1640 medium with 10% FBS. When A549 cells were at the exponential phase, the supernatants were discarded, and the cells were washed twice by serum-free medium. Then, 300 nM FAM-labeled AMO formulations in serum-free medium were added to each well, followed by incubation for 4 h at 37°C. The cells were then washed 3 times with 1 mL of PBS, and fixed with 4% ice-cold paraformaldehyde for 10 min. For nuclei staining, the cells were incubated with DAPI (Roche, USA) for 10 min at room temperature. Cellular fluorescence was visualized using a Leica TCS SP2 Confocal Laser Scanning Microscope (CLSM, Germany).

Flow cytometry analysis of A549 cells transfected by labeled AMO formulations was performed, as well. The transfected cells were treated by trypsin and subjected to centrifugation (200 g, 5 min). After removal of the supernatant, the cell pellets were washed twice with PBS and resuspended in 1 mL 70% ethanol overnight. On the other day, ethanol was replaced by PBS for flow cytometry. The intensity of fluorescein-labeled AMO in A549 cells was determined by gating cells at an excitation wavelength of 488 nm using an argon ion laser (FACS Canto™ II, BD, USA).

Effects of AMO-CLOSs on Cell Proliferation

Cell viability of A549 cells was determined by MTT assay. The cells were plated in 96-well culture plates at a density of 1×10^4 cells/well and incubated for 24 h at 37°C prior to drug treatments. The following day, cells were transfected in triplicate with AMO-CLOSs for 4 h with a series concentration of miR-21 AMO (50–500 nM). After AMO-CLOSs transfection, A549 cells were re-fed with RPMI 1640 supplemented with 10% FBS for a further 72-h culture. Then, a measure of 20 μL of MTT solution (5 mg/mL) was added to each well. In the absence of light, samples were incubated for 4 h, and precipitates were resuspended by adding 150 μL of DMSO to each well in order to ensure solubilization of the formazan crystals. Cell viability was assessed by measuring the absorbance at 570 nm with a microplate reader (Model 550, Bio-Rad, USA).

In addition, to test the sequence specificity of AMO, we introduced AMO with 3 nt mismatched to miR-21 (5′-TCATGATCAGACTGATAAGCTA-3′, 3MM AMO) and scrambled AMO control (5′-GGAAGTAAG GACCAGAGACAAA-3, control AMO) into MTT assay and the following experiments. 3MM AMO-loaded SLNs (3MM-CLOSs) and scrambled AMO control-loaded SLNs (Control-CLOSs) were prepared as mentioned above.

Apoptosis Analysis

Propidium iodide (PI) staining was carried out to identify the induction of apoptosis in A549 cells treated with different AMO formulations. A549 cells were plated in a 12-well plate and incubated overnight. At 72 h after AMO treatment, cells were collected and washed with PBS, followed by suspension in 70% ice-cold ethanol overnight for subsequent experiments. After treating with RNase A (50 μg/mL, Sigma, USA), the cells were stained with propidium iodide (100 μg/mL, Sigma) in 0.1% TritonX-100 solution for 30 min. Then the cells were analyzed for apoptosis using flow cytometry (FACS Canto™ II, BD, USA), and those in sub-G1 phase were considered as apoptotic cells.

Real-Time PCR-Based Detection of miR-21 Level

The RealMasterMix (SYBR Green) qRT-PCR miRNA Detection Kit (TianGen, Bejing, China) was used in

conjunction with SYBR Green I for quantification of miRNA transcripts in our study. A549 cells were treated with AMO formulations and incubated for further 2 days. Total RNA was extracted from cells using the RNA isolation kit (TianGen) and stored at −70°C until use. For RT reactions, ~50 ng of total RNA were subjected to reverse transcription with the sequence-specific stem-loop RT primers for miR-21 (RiboBio, Guangzhou, China) to generate the first-strand cDNA. Then the cDNA products were diluted at 2.5×, and 2 μL of the diluted cDNA was used for SYBR Green-quantitative real-time PCR reaction along with miRNA primers. Subsequently, this PCR reaction was conducted at 95°C for 3 min followed by 40 cycles of 95°C for 10 s, 60°C for 20 s and 70°C for 10 s on the iQ™5 Real-Time PCR Detection System (Bio-Rad, USA). The expression of mature miR-21 was analyzed and normalized using the $2^{-\Delta\Delta Ct}$ method (27) relative to U6 small nuclear RNA (snRNA). The change in miRNA expression was calculated as the fold variation, i.e. relative to the untreated control.

Cell Motility and Invasion Assays

After transfecting with anti-miR-21 AMO and AMO-CLOSs, A549 cells were collected for 24-well transwell migration and invasion assays. For the migration assay, briefly, A549 cells were washed with PBS, followed by resuspending in the serum-free medium, and 1×10^5 cells were allowed to migrate in the upper chambers (8 μm pore size of the polycarbonate membrane; Coring, USA). The lower chambers were filled with 0.6 mL of RPMI-1640 medium containing 20% serum as a chemoattractant. After the cells were incubated for 24 h at 37°C in a humidifed incubator with 5% CO_2, the migrated cells were fixed with 100% ice-cold methanol for 20 min and stained with Giemsa (Sigma, USA) solution (1: 9 in PBS, pH 6.8).

Similarly, transwell invasion assay was performed in 24-well ECMgel-coated chambers. The transfected cells were seeded on the ECM gel-coated membrane (8 μm pore size) with subsequent procedures same with the migration assay. The migrated and invasive cells on the lower surface of the membrane were counted in three different fields per well, and the images were captured under a microscope.

Statistical Analysis

Values were expressed as the mean ± standard error from at least three separate experiments performed in triplicate, unless otherwise noted. The differences/correlations between two groups were analyzed using Student's *t*-test, as appropriate, with a 0.05 level of significance.

RESULTS

Formation of Hydrophobic DDAB-AMO Complexes

For the binding reaction between AMO and lipid, a certain amount of AMO was extracted using 0–120 nmol cationic lipid DDAB through a Bligh and Dyer monophase. During the procedure, most AMO migrated into the chloroform solution from the aqueous phase due to the formation of hydrophobic DDAB-AMO complexes. It is the conclusion that the electrostatic interaction between the cationic head group of the lipid and the negatively charged AMO drives the formation of the complexes. In our study, the effects of the DDAB amounts on the binding efficiency were measured by a fluorescent method. The binding efficiency was calculated as AMO in the organic phase/total AMO. The results presented in Fig. 2 illustrated that increasing DDAB resulted in an increase in the binding efficiency between AMO and DDAB. Specifically, when 60 nmol of DDAB, a monovalent cationic lipid, was added to 10 μg of AMO, 93.8% of the AMO was extracted into the organic phase. When the amount of DDAB reached 90 nmol, a slight amount of AMO was recovered in the aqueous phase, and the binding efficiency was 99.2%.

Characterization of AMO-CLOSs

Solid lipid nanoparticles (SLNs) loaded with hydrophobic DDAB-AMO complexes (AMO-CLOSs) were prepared by a solvent diffusion method. Solid lipid glyceryl monostearate, cholesterol and SPC, and hydrophobic DDAB-AMO complexes were first dissolved in ethyl acetate to form oily phase followed by dispersion in the outer aqueous phase. Then the O/W emulsion was subjected to evaporation.

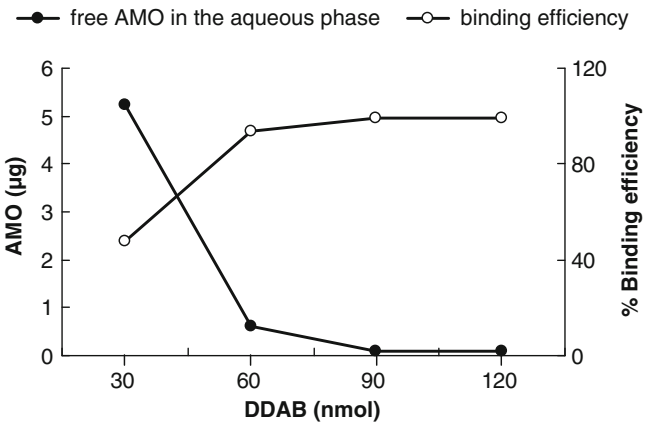

Fig. 2 Effect of increasing amounts of DDAB on the recovery of AMO in the aqueous phase and on the DDAB-AMO binding efficiency following Bligh and Dyer extractions. The amount of FAM-labeled AMO was 10 μg.

Dynamic light scattering (DLS) and zeta-potential measurements showed that nanoparticles in an average size of 187.0±2.6 nm were obtained with the polydispersity value of 0.108±0.032 and zeta potential of 46.6 mV, respectively. As shown in Fig. 3, the morphological observation of AMO-CLOSs by TEM imaging displayed that the particles were toroid in shape with an average diameter of 200 nm approximately.

In the preliminary tests, hydrosoluble AMO was added to an inner aqueous phase to prepared W/O/W double emulsion followed by formation of SLNs, while the incorporated efficiency of AMO was as low as ~20%. In order to improve the adsorption of hydrosoluble AMO into liposoluble solid lipid matrix, hydrophobic DDAB-binded AMO complexes were prepared at first. As a consequence, the encapsulation efficiency of AMO-CLOSs was 83.42±0.3%.

Hybridization Capability of Loaded Anti-microRNA-21 AMO

In the degradation experiment, AMO-CLOSs were subjected to DNase I (2.5 U/μg AMO) to investigate their ability to protect AMO from enzymatic degradation. The hybridization capability of AMO was represented in terms of melting curves (T_m value). The T_m value of degraded oligonucleotides would be lower than that of integrated ones (26), so in our study, the stability was assessed by the hybridization capability of AMO. As shown in Fig. 4, at different time intervals, the T_m value of AMO in AMO-CLOSs groups was kept in a temperature range which could be detected under the melting curve. AMO remained stable when incorporated in AMO-CLOSs even if they were subjected to the enzymatic digestion overnight (T_m maintained at 56.71°C). However, the T_m value of free AMO was 55.18°C in the first 5 min, but it was undetectable after 0.5 h treatment with DNase I, suggesting that free AMO lost its hybridization capability at 0.5 h.

Cellular Uptake of AMO-CLOSs

In order to investigate the ability of SLNs to carry genes into cells, the cell internalization of fluorescent AMO-CLOSs was assayed by CLSM and flow cytometry (Figs. 5 and 6). In CLSM images, green fluorescence for FAM-labeled AMO marker and blue flurescence for DAPI staining of the nuclei were visualized. As can be seen in Fig. 5, a visible fluorescence intensity of lipofectamin™ 2000-AMO complexes (lipo-AMO) or AMO-CLOSs within the cells was observed at 37°C, most of which were localized in the cytosolic compartment and the nuclei. However, very little FAM fluorescence was detected in the cells after incubation with free AMO. It was indicated that SLNs could promote the cellular internalization of hydrosoluble AMO. To investigate the uptake amount of AMO, we also carried out flow cytometry in this experiment, and the results are shown in Fig. 6. Intracelluar uptake of AMO-CLOSs and lipo-AMO was higher than that of free AMO. Compared with free AMO group, more transfection efficiency in lipo-AMO (81.1%) and AMO-CLOSs (74.6%) groups was observed by flow cytometry (Fig. 6a). The uptake in terms of the mean fluorescence intensity (MFI) value of AMO-CLOSs was significantly higher than that of free AMO ($P<0.001$). In addition, there was no significant difference in the MFI values between the AMO-CLOSs group and the lipo-AMO group ($P>0.05$).

Cell Viability

Cell proliferation was assessed by MTT assay. To test the sequence specificity of AMO, the effects of several SLN formulations (AMO-CLOSs, 3MM-CLOSs and Control-CLOSs) on the A549 cell death were examined simultaneously. As negative controls, mock group (all reagents except for AMO), 3MM-CLOSs, Control-CLOSs and free AMO were used. Conversely, the positive control was lipo-AMO. Cells were treated with

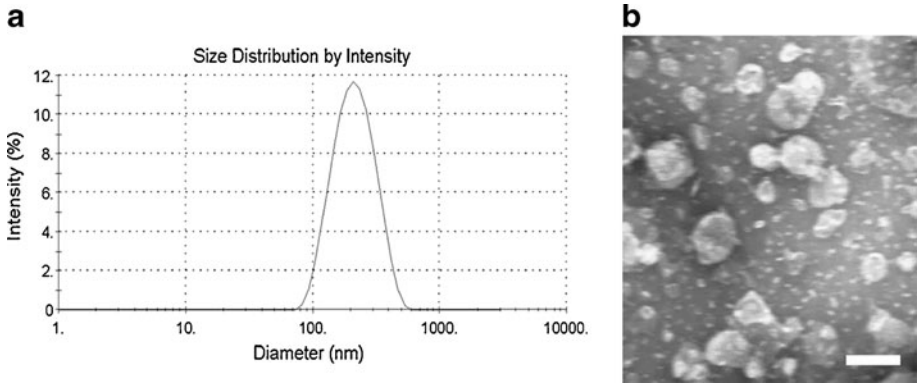

Fig. 3 Morphology and size distribution of AMO-CLOSs. (**a**) The size distribution of AMO-CLOSs by intensity, (**b**) TEM image of AMO-CLOSs (1% phosphotungstic acid-negative staining; Scale bar: 200 nm).

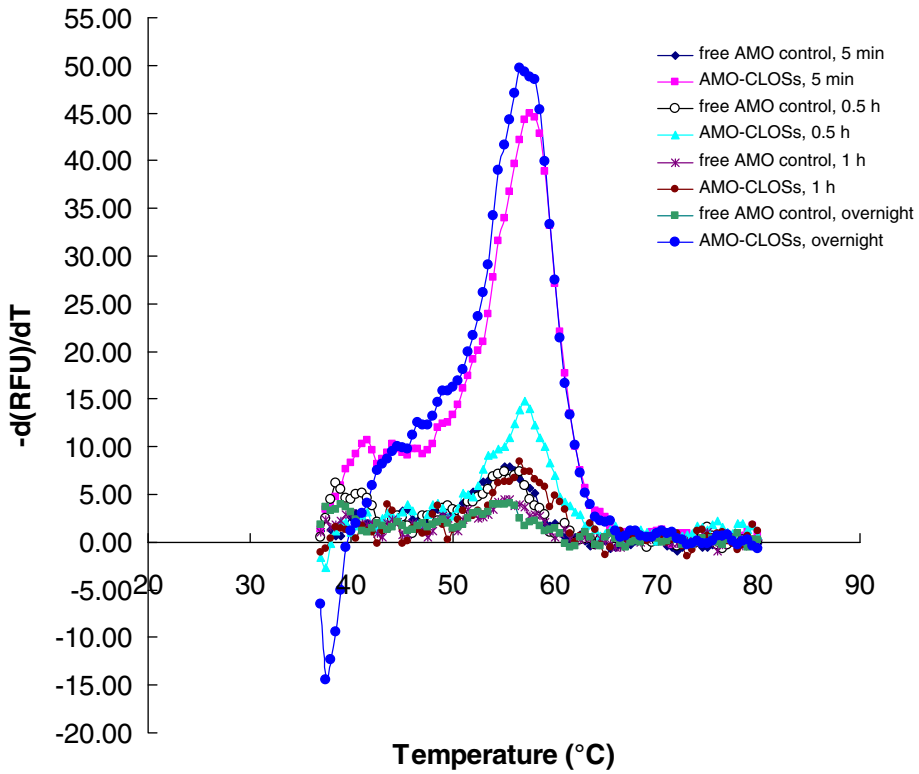

Fig. 4 Fluorescence melting curve (T_m value) analysis of AMO after treatment with DNase I. The T_m value of oligonucleotide was decreased when it was degraded by enzymatic digestion; therefore, the stability of AMO after enzyme treatment could be assessed by hybridization capability.

the same concentrations of control groups and nanoparticulate AMO ranging from 50 to 500 nM (equal to nM of AMO). At low doses of AMO, the cell growth did not change much (Fig. 7). But in the case of AMO-CLOSs and lipo-AMO at 200 nM concentration, the cell proliferation was decreased quickly compared to four negative control groups ($P<0.05$). When the concentrations were increased to 300 and 500 nM, this phenomenon of decreasing was more visible ($P<0.05$). However, considering the cytotoxicity of the nanoparticle-forming material such as DDAB, we chose 300 nM of AMO-CLOSs for AMO delivery as their effective dose against A549 cell growth. In addition, the AMO-CLOSs group showed no significant difference with the lipo-AMO group ($P>0.05$). 3MM-CLOSs and Control-CLOSs showed no effects on the cell growth compared with AMO-CLOSs at the same concentration.

Cell Apoptosis and Necrosis

Cell apoptosis analysis of A549 cells is shown in Fig. 8. It was easy to find that apoptotic peaks (sub-G_1 peaks) appeared in both AMO-CLOSs and lipo-AMO groups. Among the four negative control groups, the proportions of cells in sub-G_1 peaks were 3.1% (mock), 4.6% (3MM-CLOSs), 4.1% (Control-CLOSs) and 4.2% (free AMO), respectively. In comparison, after treating with AMO-CLOSs at 48 h-post *in vitro* culture, the proportion of apoptotic and necrotic cells gave rise to a mean of 21.0% ($P<0.05$, *vs.* negative controls) in sub-G_1 phase, which was a few lower than that of the group treated with lipo-AMO (positive control, 24.8%) ($P>0.05$).

Antisense Effect of Mature MicroRNA-21

MiR-21 silencing in cancer cells induces cell apoptosis and arrests cell proliferation (7,12,13). After the treatment of AMO formulations, we analyzed the expression of apoptosis-related miR-21, which was normalized to U6 snRNA. First of all, the melting-curves of miR-21 and U6 were sharply defined curves with a narrow peak, which indicated that pure and specific products were produced (Fig. 9a). The relative expression of miRNA-21 in negative controls was markedly higher than that in the positive control group or AMO-CLOSs group ($P<0.05$, Fig. 9b), indicating that AMO delivered into cells could reduce the miR-21 level. If the miR-21 expression of untreated A549 cells was normalized as 1.00, the relative expressions of miR-21 in lipo-AMO and AMO-CLOSs groups were 0.77 and 0.71, respectively. Compared with the mock group, the AMO-CLOSs group had a 1.52-fold repression of miR-21, and the lipo-AMO group had a 1.40-fold repression of miR-21, suggesting that anti-miR-21 AMO in SLNs could down-regulate the expression of mature microRNA-21 in A549 cells. Meanwhile, on the electrophoresis gel, the miR-21

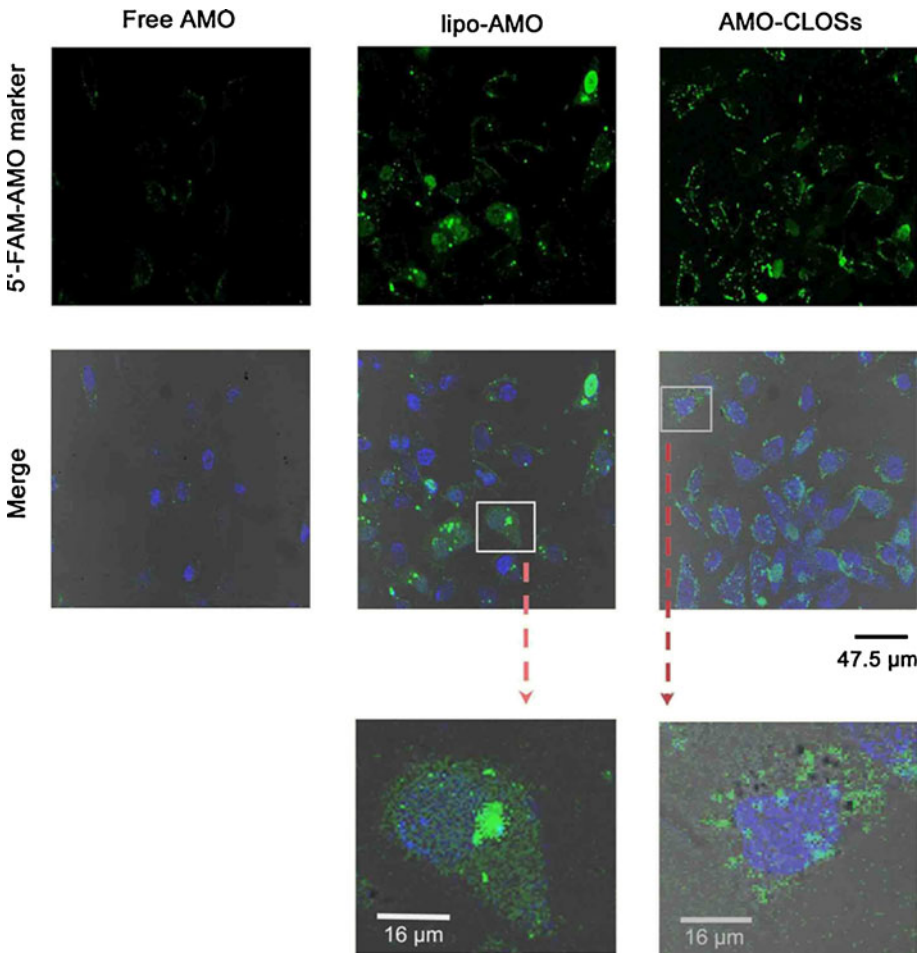

Fig. 5 Confocal laser scanning microscopy images of intracellular distribution of FAM-labeled AMO-CLOSs and naked FAM-AMO in A549 cells. (*green fluorescence*, FAM-AMO marker; *blue fluorescence*, nucleus)

PCR products of AMO-CLOSs-treated A549 cells were less than those of the negative controls (Fig. 9c).

Suppression in Cell Migration and Invasion

Next, we determined whether the transfection of A549 cell line with AMO-CLOSs could affect the cell migration and invasion. After the treatment with Transwell assay, cells on the upper surface of the filter were completely removed by wiping them with a cotton swab, and the migrated cells were stained by Giemsa. A549 cell migration was suppressed significantly ($P<0.05$), and approximately 55.4% and 55.9% reduction in migratory tendency was observed in cells treated with lipo-AMO and AMO-CLOSs, respectively (Fig. 10a). In the other four groups, however, the high cell migration efficicency was found. Simultaneously, cell migration was not altered significantly by the transfection of A549 with SLNs loaded with 3 nt mismatched AMO or scrambled AMO.

In parallel, we also determined the effect of AMO-CLOSs on cell invasion across an extracellular matrix of ECM gel. Consistent with the cell migration study, the results of cell invasion were shown in Fig. 10b. The AMO-CLOSs-transfected cells showed a significant reduction in invasion, while 3MM-CLOSs or Control-CLOSs had no influence on cell invasion, suggesting that a sequence specificity existed in the functional role of anti-miR-21 AMO. In addition, the invasion index of A549 cells decreased to 43.6% (lipo-AMO) and 53.1% (AMO-CLOSs), respectively, whereas the four negative controls failed to show a significant effect (~100%) ($P<0.05$). These results indicated that SLNs (CLOSs) efficiently delivered AMO into cells to depress cell migration and invasion.

DISCUSSION

Understanding of miR-21 functions is of great help for exploiting a new potential therapeutic target for human cancer. Since miR-21 may act as an oncogene in the lung cancer, we introduced anti-miR-21 AMO to suppress its function, followed by facilitation of cell apoptosis. The

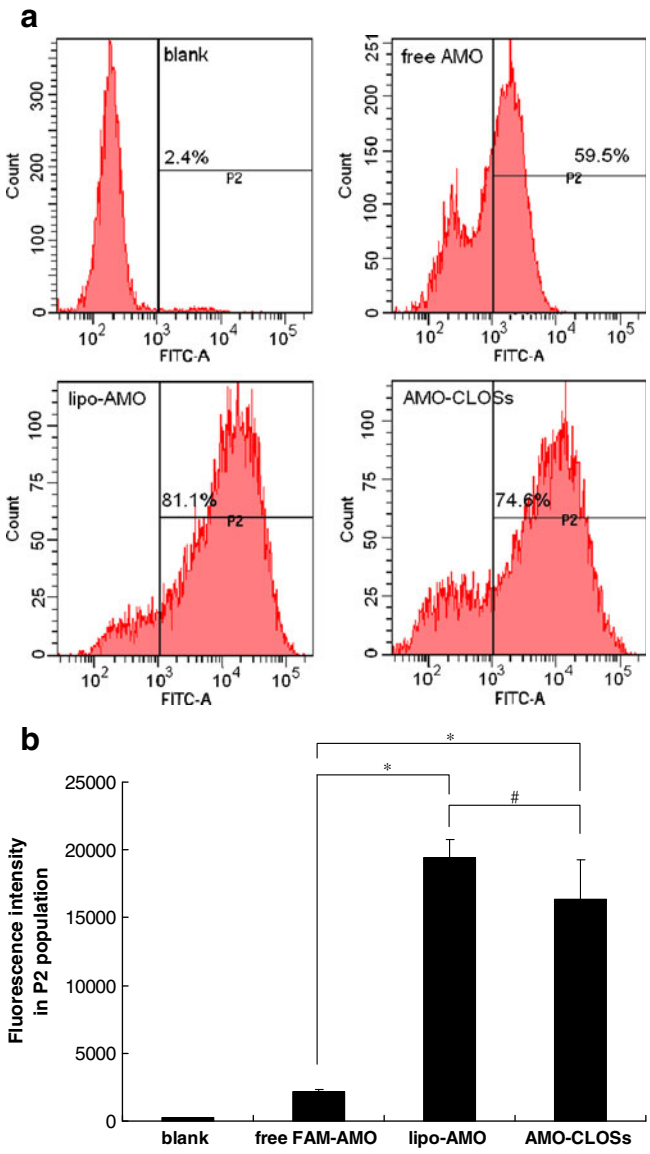

Fig. 6 Flow cytometry analysis of *in vitro* uptake of FAM-AMO-CLOSs by A549 cells. (**a**) The histogram of AMO formulations was measured by flow cytometry. (**b**) The mean fluorescent intensity in P2 population of different AMO formulations associated with the cells was measured following 4 h incubation at 37°C. P2, the positive cells transfected by FAM-labeled formulations. Each value represents the mean ± S.D. of three experiments. Statistically significant differences (*$P < 0.001$) from the control of free FAM-AMO. # $P > 0.05$, not significant with lipo-AMO group.

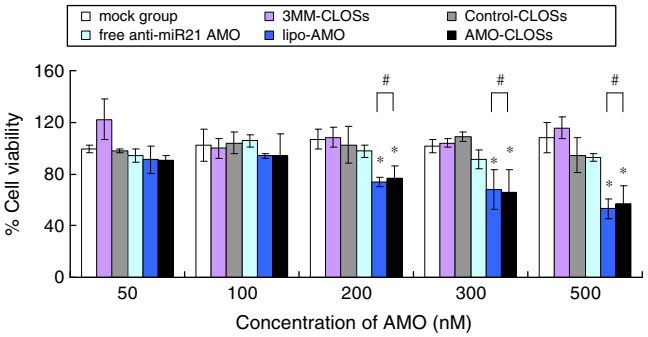

Fig. 7 Cell viability of AMO formulations by MTT assay. Mock group (all reagents except for AMO), 3 nt mismatches of AMO in SLNs (3MM-CLOSs), scrambled AMO control oligonucleotides in SLNs (Control-CLOSs), free anti-miR-21 AMO were carried out as negative controls, and lipofectamin™2000-AMO complexes (lipo-AMO) was the positive control. MTT assay was measured in triplicates at 72 h. (*$P < 0.05$, compared with mock, 3MM-CLOSs, Control-CLOSs and free anti-miR-21 AMO group, respectively; # $P > 0.05$, compared with lipo-AMO group)

essence of AMO is an oligonucleotide sequence, with poor stability and weak intracellular penetration. Carriers are necessary to overcome this; therefore, how to develop an efficient delivery vehicle for AMO to protect it from degradation and increase the transport efficiency across the cell membrane is critical for antisense microRNA therapeutics. The most common systems to combine DNA for gene delivery involve liposomes (28,29) or polymers (30,31), both exhibiting high transfection efficiencies. Nevertheless, this research is far from final completion, and some drawbacks hold back further use because of the poor stability or potentially toxic/allergic materials used. Simultaneously, even if the cationic liposomes and polymeric carriers and SLNs are promising nonviral delivery systems with high transfection efficiency, the association with miRNA-based therapeutics of these nonviral vectors has been somewhat ignored. In this study, solid lipid nanoparticles loaded with anti-microRNA oligonucleotides (AMO-CLOSs) were tested for the first time for the high delivery capability and enhanced efficiency over their naked forms. SLN carriers are made from the natural lipid materials and show high uptake capacity for anticancer drug delivery *in vitro* (19,25,32) and also protect nucleic acids from degradation (20), as well as posses good stability. As expected, AMO-CLOSs, composed of cationic and solid lipids and associated with miRNA-based therapeutics effectively delivered AMO, which then inhibited mature miR-21 expression in A549 cells.

Generally, the SLNs-DNA complexes were obtained by incubating SLNs with DNA for a certain time (20,22), which have to be prepared right before the transfection experiment. In this study, a novel but simple preparation method was established to load AMO into SLNs. Previously, SLNs have been widely used to encapsulate lipophilic drugs with high encapsulation efficiencies (18). However, hydrosoluble drugs are difficult to incorporate into SLNs. To address this problem, the drug in terms of phospholipid complex was emerged to formulate SLNs (19), and a W/O/W double emulsion method was performed to prepare SLNs with high incorporated efficiencies (33,34). With this in mind, to improve the incorporation efficiency of hydrosoluble AMO in SLNs, DDAB-AMO complexes (lipid-drug binding complexes, LDC) with high lipophilicify were

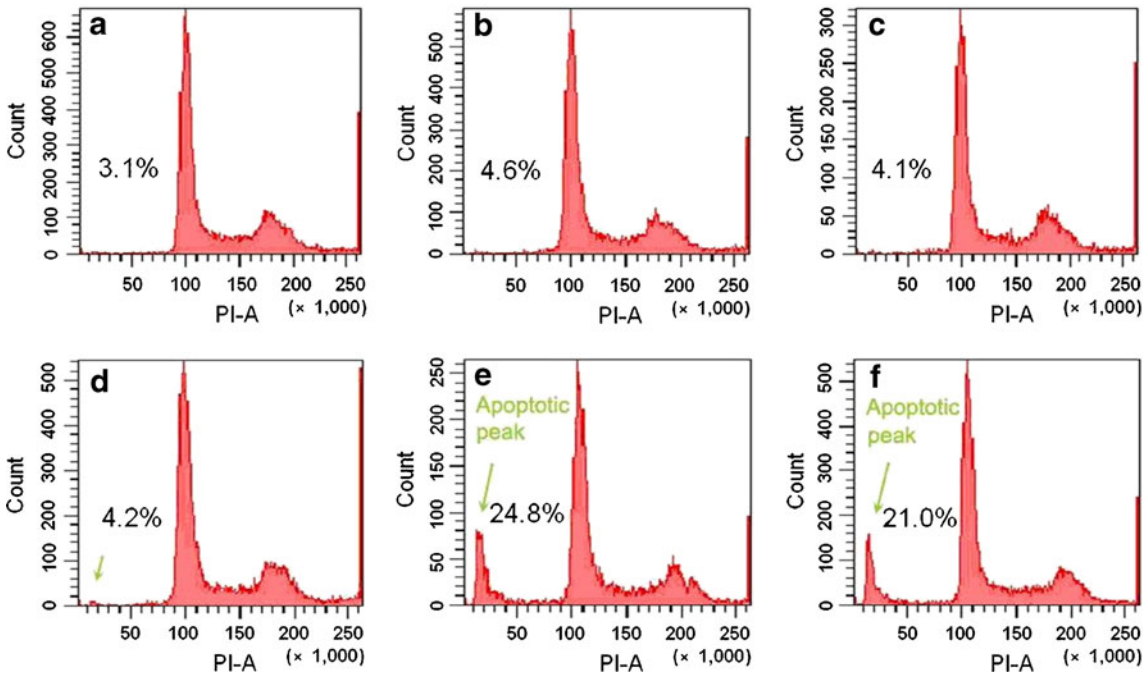

Fig. 8 Induction of cell apoptotis by AMO-CLOSs in A549 cells. The treated cells were subjected to propidium iodide (PI) staining, and apoptotic cells and necrotic cells were analyzed by flow cytometry. (**a**) Mock; (**b**) 3MM-CLOSs; (**c**) Control-CLOSs; (**d**) free anti-miR-21 AMO; (**e**) lipo-AMO; (**f**) AMO-CLOSs.

prepared initially by bligh and dyer extraction. Then the complexes were solved in the oily phase to form SLNs. To our knowledge, this was the first report to load AMO into SLNs by this method. DDAB-AMO complexes, distributed in chloroform phase, were in formation for the electrostatic interaction between negatively charged AMO and positively charged DDAB. A potent colloid system of AMO-CLOSs was finally obtained (Fig. 1) with a postulated structure that glyceryl monostearate constituted the solid core and SPC acted as phospholipid shell coating the particle. Lipophilic LDC was located in the core of SLNs. For this SLN system, as high as a 83.42% of encapsulation efficiency for AMO was achieved with 187 nm in size and 46.6 mV in zeta potential, which might be beneficial to the cell absorption. More importantly, AMO-CLOSs protected AMO from digestion by DNase as compared to the free AMO, which was accessible to enzymatic attack (Fig. 4).

SLNs have been proven to have high uptake efficiencies by cells (19,25,32,35). After the formulation was optimized, fluorescent AMO-CLOSs were subjected to the cell internalization experiments, which showed a similar transfection efficiency comparable with the commercially available lipofectamine™ 2000 (Figs. 5 and 6). However, significantly higher transfection of FAM-labeled AMO-CLOSs was visualized in lung cancer cells compared with that of the free AMO. It may be partially attributed to the tenacious affinity of the helper lipid SPC to the cells (19). Moreover, DDAB donated its partial positive charge to the surface of AMO-CLOSs, which facilitated the interaction with cell membrane and enhanced the cell permeability and the subsequent transfection efficiency (36). Therefore, in contrast to the free AMO group, fluorescent marker of AMO-CLOSs group was more diffuse distributed over the cytoplasm and the nucleus at 37°C. These features indicate that AMO-CLOSs are adequate for association with the negatively charged cell membrane and subsequent internalization into the cells.

After internalization, AMO in such intracellular compartment could correct the aberrant activity of miR-21-mRNA interaction (14). Therefore, AMO-CLOSs would provide a means to introduce anti-miR-21 AMO into cells to achieve maximal cellular therapeutic benefit, decreasing the amount of drug required and accomplishing the specific silencing of mature miR-21. As can be seen from the results of pharmacodynamic studies *in vitro* (Figs. 7, 8, 9 and 10), AMO-CLOSs with a high transfection significantly inhibited cell proliferation and promoted cell apoptosis. QRT-PCR analysis indicated that AMO-CLOSs reduced the cellular level of miR-21, and Transwell assay proved that AMO-CLOSs-treated A549 cells were attenuated in cell motility and invasion. In contrast, naked AMO-treated cells with low transfection showed little effect on silencing of overexpressed miR-21. For this reason, it may be supposed that the higher transfection of AMO-CLOSs in lung cancer cells seems to be responsible for the higher silencing effect

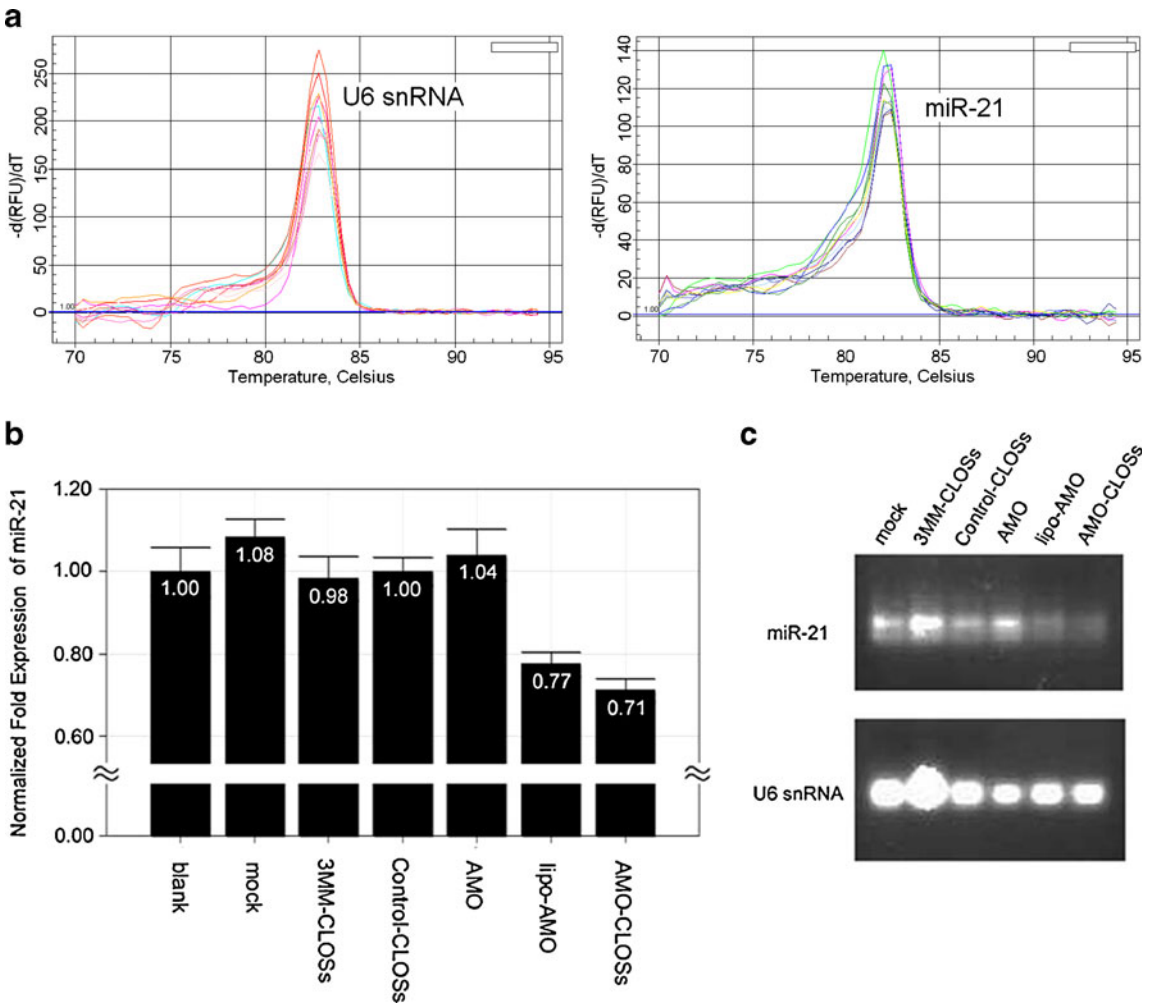

Fig. 9 Quantitative real-time PCR analysis and electrophoresis gel analysis of miR-21 level in A549 cells. Inhibited expression of miR-21 in A549 cells using AMO-CLOSs and its positive control. The expression of miR-21 was normalized to U6 small nuclear RNA gene (U6 snRNA) control. The blank was untreated A549 cells without any other process. (**a**) The melting-curves (T_m value) of miR-21 and U6 were presented as a single peak. (**b**) Expression of miR-21 was detected by quantitative real-time PCR. (**c**) MiR-21-specific products were amplified by qRT-PCR from the cDNAs derived from treated A549 cells, then data were grouped according to the intensity of the obtained signals of the product bands on agarose gels.

of miR-21, which modulates the tumor suppressor genes, e.g. PTEN, PDCD4 and Tropomyosin 1 (TPM1), relative to cell proliferation, migration and invasion (7–9,37). In agreement with this, the suppressing of miR-21 functionally involved in PTEN/PDCD4/TPM1-dependent pathways of A549 cell growth, migration and invasion as a consequence of the correlative protein knock-down. The *in vivo* phenotypic characteristics (not examined here) of AMO-CLOSs in solid tumors are necessary to assess the application of AMO-CLOSs. However, such highly cationic lipid used in the nanoparticles would be potentially toxic *in vivo* and may cause potential problems associated with *in vivo* application of the SLNs. To overcome these challenges a further-optimized formulation with less cationic lipids can reduce the toxicity, and specific ligand-modified SLNs are conceivable for their selective targeting.

On the other hand, the sequence-specific AMO is required for anti-miR-21 fuction (10). Mismatch specificity was tested by 3 nt mismatches AMO and scrambled AMO control. As shown in Figs. 7, 8, 9 and 10, AMO with 3 nt mismatches to miR-21 in SLNs failed its activity as well as the scrambled AMO. These results suggest that anti-miRNA AMO is likely to be specific for individual miRNA family members.

CONCLUSIONS

In conclusion, AMO-CLOSs were prepared as a colloidal system for miRNA-based therapeutics. As expected, they have been proven to be efficient for protecting the integrality of AMO from degradation and increasing the intracellular transfection. In addition, AMO-CLOSs effec-

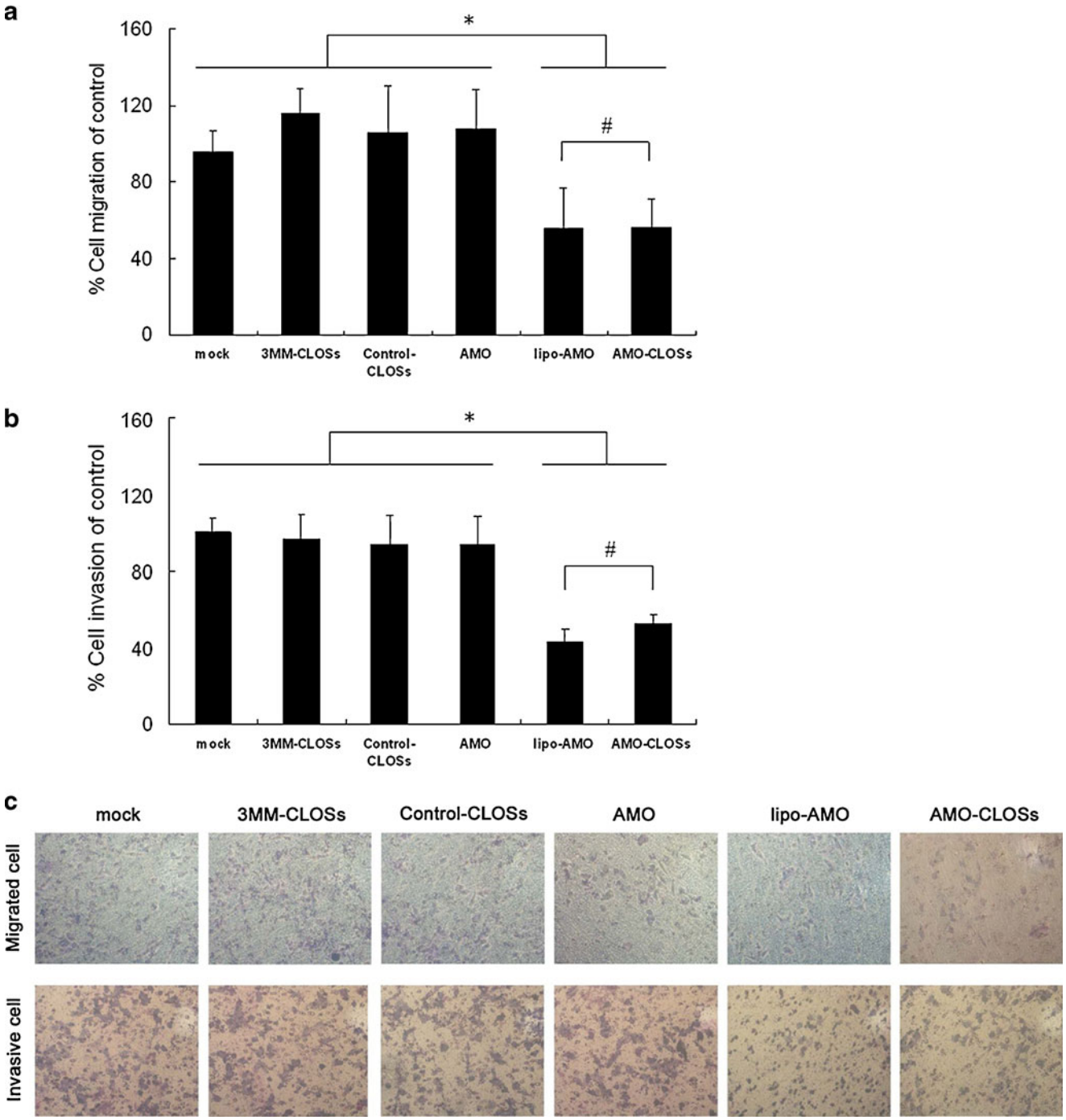

Fig. 10 The anti-miR-21 effects of AMO-CLOSs on A549 cell migration and invasion using Transwell assay. Migrated or invasive cells across the membrane or the ECM gel-coated membrane with 8-μm pores were assessed as described in the "Materials and Methods" section. (**a**) The relative percentage of cell migration was summaried with non-transfected control, and the average rate of migrated cells were from three independent experiments ± SD. (*$P < 0.05$, compared with mock group, 3MM-CLOSSs, Control-CLOSSs and free anti-miR-21 AMO group; # $P > 0.05$, compared with lipo-AMO group) (**b**) The relative percentage of cell invasion was summaried with non-transfected control, and the average rate of invasion cells were from three independent experiments ±SD. (*$P < 0.05$, compared with mock group, 3MM-CLOSSs, Control-CLOSSs and free anti-miR-21 AMO group; # $P > 0.05$, compared with lipo-AMO group) (**c**) Representative fields of migrated and invasive cells on the membrane. Cells were stained by Giemsa into brown (magnification, ×200).

tively deliver AMO into cells for silencing over-expressed miR-21 as a result of inducing cell growth and apoptosis, and bringing down cell migration and invasion. Thus, our delivery system of AMO with AMO-CLOSSs is a promising and potential therapeutic strategy for lung cancers associated with the abnormal expression of microRNA.

ACKNOWLEDGMENTS & DISCLOSURES

This present study is supported by the National Natural Science Foundation of P.R.China (No. 30873165) and the National Science & Technology Major Project of China (No. 2009ZX09310-002).

REFERENCES

1. Bartel DP. MicroRNAs: genomics, biogenesis, mechanism, and function. Cell. 2004;116:281–97.
2. Lu J, Getz G, Miska EA, Alvarez-Saavedra E, Lamb J, Peck D, *et al.* MicroRNA expression profiles classify human cancers. Nature. 2005;435(9):834–8.
3. Ambros V. The functions of animal microRNAs. Nature. 2004;431:350–5.
4. Gregory RI, Shiekhattar R. MicroRNA biogenesis and cancer. Cancer Res. 2005;65(9):3509–12.
5. Hammond SM. MicroRNAs as oncogenes. Curr Opin Genet Dev. 2006;16:4–9.
6. Volinia S, Calin GA, Liu CG, Ambs S, Cimmino A, Petrocca F, *et al.* A microRNA expression signature of human solid tumors defines cancer gene targets. Proc Natl Acad Sci USA. 2006;103(7):2257–61.
7. Zhang JG, Wang JJ, Zhao F, Liu Q, Jiang K, Yang GH. MicroRNA-21 (miR-21) represses tumor suppressor PTEN and promotes growth and invasion in non-small cell lung cancer (NSCLC). Clin Chim Acta. 2010;411(11–12):846–52.
8. Frankel LB, Christoffersen NR, Jacobsen A, Lindow M, Krogh A, Lund AH. Programmed cell death 4 (PDCD4) is an important functional target of the microRNA miR-21 in breast cancer cells. J Biol Chem. 2008;283:1026–33.
9. Zhu S, Si ML, Wu HL, Mo YY. MicroRNA-21 targets the tumor suppressor gene tropomyosin 1 (TPM1). J Biol Chem. 2007;282 (19):14328–36.
10. Davis S, Lollo B, Freier S, Esau C. Improved targeting of miRNA with antisense oligonucleotides. Nucleic Acids Res. 2006;34 (8):2294–304.
11. Ørom UA, Kauppinen S, Lund AH. LNA-modified oligonucleotides mediate specific inhibition of microRNA function. Gene. 2006;372:137–41.
12. Fei J, Lan FE, Guo M, Li YM, Liu Y. Inhibitory effects of anti-miRNA oligonucleotides (AMOs) on A549 cell growth. J Drug Target. 2008;16(9):688–93.
13. Hiyoshi Y, Kamohara H, Karashima R, Sato N, Imamura Y, Nagai Y, *et al.* MicroRNA-21 regulates the proliferation and invasion in esophageal squamous cell carcinoma. Clin Cancer Res. 2009;15(6):1915–22.
14. Weiler J, Hunziker J, Hall J. Anti-miRNA oligonucleotides (AMOs): ammunition to target miRNAs implicated in human disease? Gene Ther. 2006;13:496–502.
15. Hughes MD, Hussain M, Nawaz Q, Sayyed P, Akhtar S. The cellular delivery of antisense oligonucleotides and ribozymes. Drug Discov Today. 2001;6(6):303–15.
16. Müller RH, Mäder K, Gohla S. Solid lipid nanoparticles (SLN) for controlled drug delivery—a review of the state of the art. Eur J Pharm Biopharm. 2000;50(1):161–77.
17. Mühlen A, Schwarz C, Mehnert W. Solid lipid nanoparticles (SLN) for controlled drug delivery-drug release and release mechanism. Eur J Pharm Biopharm. 1998;45:149–55.
18. Helgason T, Awad TS, Kristbergsson K, McClements DJ, Weiss J. Effect of surfactant surface coverage on formation of solid lipid nanoparticles (SLN). J Colloid Interf Sci. 2009;334:75–81.
19. Wei W, Shi SJ, Liu J, Sun X, Ren K, Zhao D, *et al.* Lipid nanoparticles loaded with 10-hydroxycamptothecin–phospholipid complex developed for the treatment of hepatoma in clinical application. J Drug Target. 2010;18:557–66.
20. Pozo-Rodíguez AD, Delgado D, Solinís MA, Gascón AR, Pedraz JL. Solid lipid nanoparticles: formulation factors affecting cell transfection capacity. Int J Pharm. 2007;339:261–8.
21. Pan XG, Chen L, Liu SJ, Yang XJ, Gao JX, Lee RJ. Antitumor activity of G3139 lipid nanoparticles (LNPs). Mol Pharm. 2009;6 (1):211–20.
22. Choi SH, Jin SE, Lee MK, Lim SJ, Park JS, Kim BG, *et al.* Novel cationic solid lipid nanoparticles enhanced p53 gene transfer to lung cancer cells. Eur J Pharm Biopharm. 2008;68:545–54.
23. Vighi E, Ruozi B, Montanari M, Battini R, Leo E. Re-dispersible cationic solid lipid nanoparticles (SLNs) freeze-dried without cryoprotectors: characterization and ability to bind the pEGFP-plasmid. Eur J Pharm Biopharm. 2007;67:320–8.
24. Reimer DL, Zhang YP, Kong S, Wheeler JJ, Graham RW, Bally MB. Formation of novel hydrophobic complexes between cationic lipids and plasmid DNA. Biochemistry. 1995;34(39):12877–83.
25. Yuan H, Miao J, Du YZ, You J, Hu FQ, Zeng S. Cellular uptake of solid lipid nanoparticles and cytotoxicity of encapsulated paclitaxel in A549 cancer cells. Int J Pharm. 2008;348:137–45.
26. Arnedo A, Espuelas S, Irache JM. Albumin nanoparticles as carriers for a phosphodiester oligonucleotide. Int J Pharm. 2002;244:59–72.
27. Kenneth JL, Thomas DS. Analysis of relative gene expression data using real-time quantitative PCR and the $2^{-\Delta\Delta Ct}$ method. Methods. 2001;25:402–8.
28. Yamane I, Nishikawa M, Takakura Y. Cellular uptake and activation characteristics of naked plasmid DNA and its cationic liposome complex in human macrophages. Int J Pharm. 2005;305:145–53.
29. Fillion P, Desjardins A, Sayasith K, Lagacé J. Encapsulation of DNA in negatively charged liposomes and inhibition of bacterial gene expression with fluid liposome-encapsulated antisense oligonucleotides. Biochim Biophys Acta. 2001;1515:44–54.
30. Xiong XB, Uludağ H, Lavasanifar A. Biodegradable amphiphilic poly(ethylene oxide)-block-polyesters with grafted polyamines as supramolecular nanocarriers for efficient siRNA delivery. Biomaterials. 2009;30:242–53.
31. Jere D, Xu CX, Arote R, Yun CH, Cho MH, Cho CS. Poly(b-amino ester) as a carrier for si/shRNA delivery in lung cancer cells. Biomaterials. 2008;29:2535–47.
32. Olbrich C, Bakowsky U, Lehr CM, Müller RH, Kneuer C. Cationic solid-lipid nanoparticles can efficiently bind and transfect plasmid DNA. J Control Release. 2001;77:345–55.
33. Liu J, Gong T, Wang CG, Zhong ZR, Zhang ZR. Solid lipid nanoparticles loaded with insulin by sodium cholate-phosphatidylcholine-based mixed micelles: preparation and characterization. Int J Pharm. 2007;340:153–62.
34. García-Fuentes M, Torres D, Alonso MJ. Design of lipid nanoparticles for the oral delivery of hydrophilic macromolecules. Coll Surf B: Biointerf. 2002;27:159–68.
35. Pedersen N, Hansen S, Heydenreich AV, Kristensen HG, Poulsen HS. Solid lipid nanoparticles can effectively bind DNA, streptavidin and biotinylated ligands. Eur J Pharm Biopharm. 2006;62:155–62.
36. Pan XG, Guan JJ, Yoo JW, Epstein AJ, Lee LJ, Lee RJ. Cationic lipid-coated magnetic nanoparticles associated with transferrin for gene delivery. Int J Pharm. 2008;358:263–70.
37. Vinciguerra M, Sgroi A, Veyrat-Durebex C, Rubbia-Brandt L, Buhler LH, Foti M. Unsaturated fatty acids inhibit the expression of tumor suppressor phosphatase and tensin homolog (PTEN) via microRNA-21 up-regulation in hepatocytes. Hepatology. 2009;49 (4):1176–84.